ACS Partner Journal

CHEMICAL & BIOMEDICAL IMAGING

Open Access

pubs.acs.org/ChemBioImaging

Article

3D Holo-tomographic Mapping of COVID-19 Microclots in Blood to Assess Disease Severity

Talia Bergaglio, Olena Synhaivska, and Peter Niraj Nirmalraj*

Cite This: https://doi.org/10.1021/cbmi.3c00126

Read Online

ACCESS | Metrics & More | Article Recommendations | Supporting Information

ABSTRACT: The coronavirus disease 2019 (COVID-19) has impacted health globally. Cumulative evidence points to long-term effects of COVID-19 such as cardiovascular and cognitive disorders, diagnosed in patients even after the recovery period. In particular, micrometer-sized blood clots and hyperactivated platelets have been identified as potential indicators of long COVID. Here, we resolve microclot structures in the plasma of patients with different subphenotypes of COVID-19 in a label-free manner, using 3D digital holo-tomographic microscopy (DHTM). Based on 3D refractive index (RI) tomograms, the size, dry mass, and prevalence of microclot composites were quantified and then parametrically differentiated from fibrin-rich microclots and platelet aggregates in the plasma of COVID-19 patients. Importantly, fewer microclots and platelet aggregates were detected in the plasma of healthy controls compared to COVID-19 patients. Our imaging and analysis workflow is built around a commercially available DHT microscope capable of operation in clinical settings with a 2 h time period from sample preparation and data acquisition to results.

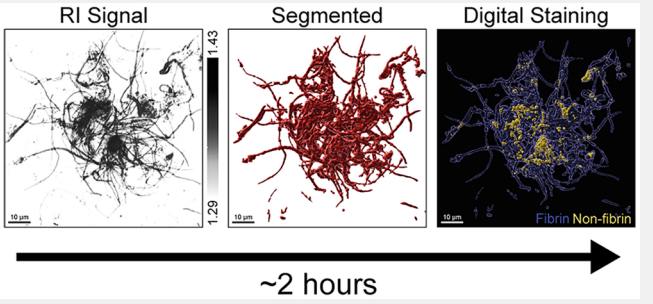

KEYWORDS: *microclots, plasma, COVID-19, long COVID, label-free imaging*

INTRODUCTION

Coronavirus disease 2019 (COVID-19) is a complex disorder caused by infection with severe acute respiratory syndrome coronavirus 2 (SARS-CoV-2) and affects many bodily functions, including excessive immunological response, autoimmunity, and endothelial dysfunction, that have been implicated in the risk of thrombotic events and coagulopathies.[1−7] While the acute phase of COVID-19 primarily manifests as a respiratory illness, with a wide range of symptoms including fever, headache, cough, fatigue, muscle pain, and shortness of breath, more severe clinical symptoms, such as systemic inflammatory response syndrome (SIRS), acute respiratory disease syndrome (ARDS), and neurological and cardiovascular complications, have been associated with processes underlying coagulopathies and endotheliopathies.[4,6,8] Currently, it is estimated that approximately 30% of individuals with COVID-19 continue to suffer from a variety of different symptoms involving specific or multiple organ systems, with neurological, neuropsychiatric, and cardiorespiratory clinical presentations,[8,9] a condition known as postacute sequelae of COVID (PASC) or long COVID.[8,10,11] Fatigue, cough, dyspnea, chest pain, headache, dizziness, cognitive impairment known as "brain fog", and long-term smell and taste dysfunction are the most commonly reported symptoms in individuals suffering from long COVID.[9,10,12] The World Health Organization defines long COVID as a condition in which individuals with a probable or confirmed infection with SARS-CoV-2 still experience COVID-19-related symptoms usually three months postinfection and lasting for at least two months, with no alternative diagnosis.[13] Endotheliopathy, coagulopathy, and thrombosis are also now established complications of COVID-19 and can persist in individuals diagnosed with long COVID, contributing to the pathogenesis and clinical manifestations of these conditions.[1,14−16]

The pathogenic mechanisms underlying coagulopathy in COVID-19 and long COVID are complex and multifactorial, including a patient's pre-existing conditions.[17,18] The presence of SARS-CoV-2 has been detected within endothelial cells, suggesting a direct viral effect on the vascular system.[19,20] Additionally, the dysregulated immune response triggered by the viral infection can lead to excessive inflammation and cytokine release, further promoting a pro-thrombotic state.[21] More specifically, COVID-19-related coagulopathy was associated with elevated levels of von Willebrand Factor (VWF), D-dimer, fibrinogen, and markers of platelet activation, as well as damaged red blood cells (RBCs) and reduced fibrinolysis, reflecting ongoing coagulation activa-

Received: December 10, 2023
Revised: December 13, 2023
Accepted: December 15, 2023

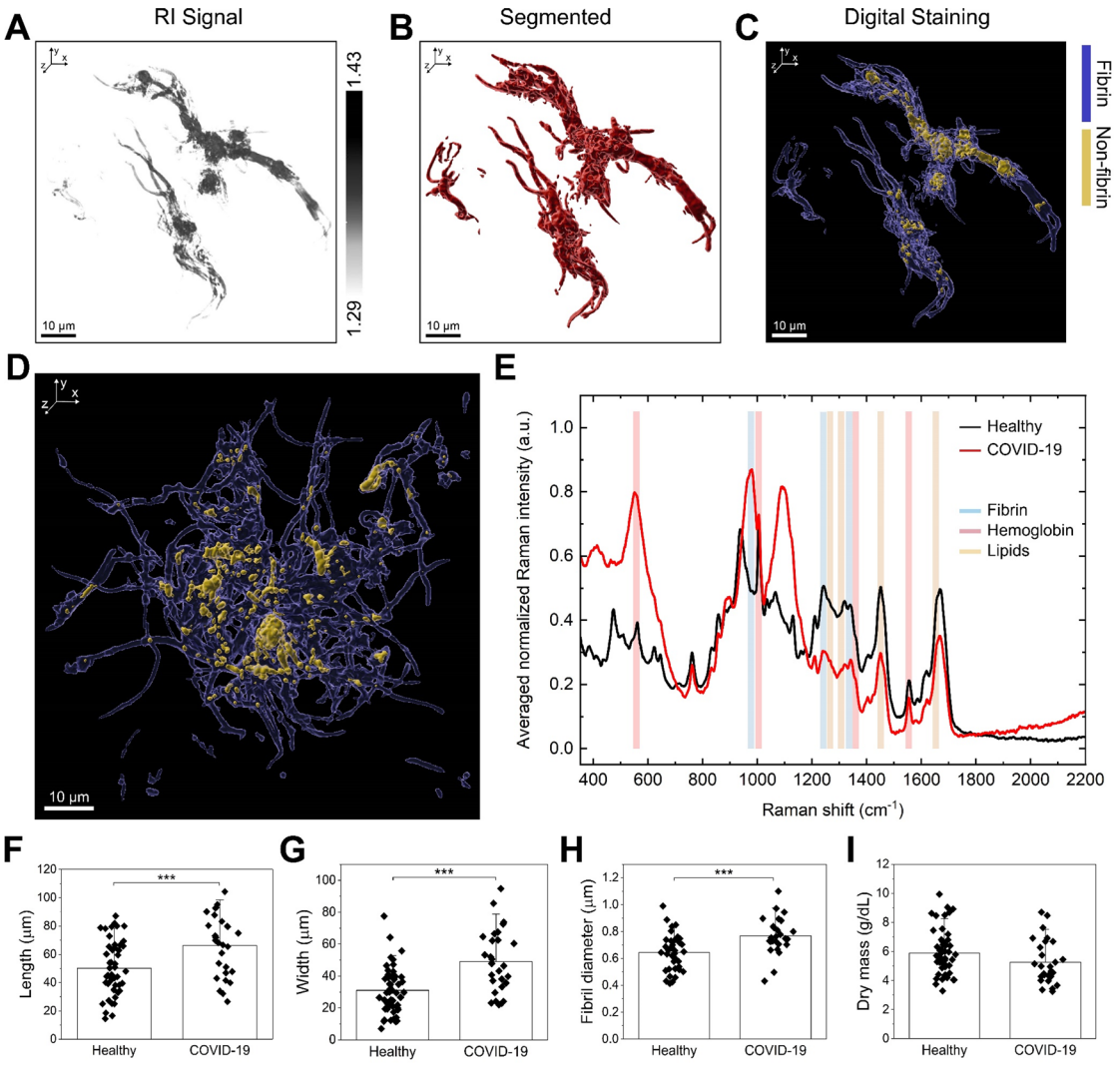

Figure 1. Structural and spectrochemical analysis of synthetically prepared fixed blood clots in aqueous solution. (A) Refractive index (RI) tomogram of a blood clot fragment obtained from a healthy donor. (B) Corresponding segmented RI tomogram and (C) digital RI staining for fibrin (blue) and non-fibrin (yellow) structures. (D) Digital RI staining for fibrin (blue) and non-fibrin (yellow) structures of a blood clot obtained from a donor with COVID-19. (E) Averaged spectral signatures of blood clots obtained from a healthy donor (black line) and a donor with COVID-19 (red line). Quantification of (F) length, (G) width, (H) fibrin fibril diameter, and (I) dry mass of blood clots from a healthy donor and a donor with COVID-19.

tion.[3,22,23] In long COVID, persistent coagulation abnormalities may contribute to the chronic and debilitating symptoms experienced by affected individuals.[1,8,24] The formation of microclots, or microthrombi, within the pulmonary vasculature has been observed, contributing to respiratory compromise.[5,25,26] The mechanisms underlying these persistent coagulation disturbances are not yet fully understood, but they may involve a combination of residual inflammation, immune dysregulation, and vascular damage.[2,5,7]

The incidence of microvascular injury in COVID-19 patients has been detected in the lungs, brain, heart, and other organs during autopsy, using magnetic resonance imaging (MRI) and upon histological examination.[24,27−29] Previously, Pretorius and co-workers[26] reported on the presence of microclots in COVID-19 platelet-poor plasma (PPP), using thioflavin T (ThT) staining and fluorescent microscopy. These microclots, ranging in size between 1 and 200 μm, were determined to be amyloidogenic, indicated by the positive ThT signal, suggesting a more anomalous clot structure characterized by extensive ß-sheet structures and presenting resistance to fibrinolysis.[4,5,20,30,31] Due to their size, microclots are known to block microcapillaries and prevent efficient oxygen transport through the blood circulation, which seems to be responsible for part, if not most of, the symptomatology in both acute and long COVID.[5,21,32]

Scanning electron microscopy and microfluidic-based studies have also provided insights into the coagulation mechanisms in COVID-19 and long COVID compared to healthy plasma by inducing blood clot formation with/without thrombin and SARS-CoV-2 spike protein.[20,33] Denser structures with thicker fibrils in the range of ∼50−150 nm in diameter were observed, in addition to increased clot rigidity and platelet hyperactivation in the COVID-19 samples. Additionally, proteomic-based analysis of microclots revealed the presence of additional plasma proteins, including VWF, complement factors, C-reactive protein, α2-antiplasmin, and the SARS-CoV-2 virus, which may induce the production of different prothrombotic autoantibodies.[3,5,33−35]

https://doi.org/10.1021/cbmi.3c00126
Chem. Biomed. Imaging XXXX, XXX, XXX−XXX

To date, evidence for the presence of microclots in the plasma of COVID-19 and long COVID patients has been mainly obtained using *in vitro* ThT staining and fluorescent microscopy.[4,9,26] Currently available diagnostic methods for the assessment of coagulopathies include qualitative assessment using ThT labeling-based fluorescent microscopy or using semiquantitative thromboelastography (TEG) and D-dimer analysis.[3−5,36] Importantly, the presence of high levels of D-dimer can serve as an indicator for the production of blood clots and subsequent adequate fibrinolysis but does not sufficiently reflect the nature, composition, and number of the residual microclots in circulation.[5] Hence, it would be highly desirable to devise a methodology that would allow for direct determination of microclot morphology, composition, and prevalence in blood in a label-free manner compatible with operating even in resource-limited clinical settings. To address this pending need, we have developed an imaging methodology based on digital holo-tomographic microscopy (DHTM) to three-dimensionally map microclot structure and composition in plasma samples from patients diagnosed with COVID-19, with high spatial resolution and in a label-free manner. In this study, we have resolved chemically fixed micrometer-size blood clots, used them as samples for optimization of imaging protocols, and then extended the DHTM-based imaging methodology to directly characterize microclots in plasma under standard laboratory conditions. No fixation protocols were used to prepare the microclots in the plasma samples.

First, the refractive index (RI) maps of synthetically prepared blood clot fragments in aqueous solution from a healthy individual and a convalescent COVID-19 patient were registered using DHTM (see Methods section for details on the clot synthesis procedure). The structural information and blood clot composition were quantified by segmenting and digitally staining the 3D RI tomograms to identify differences in size and composition between blood clot types. Raman spectroscopy measurements were also conducted to further characterize the blood clot structure and composition. Next, we extended the imaging and analysis protocols to directly examine the plasma of individuals with different COVID-19 subphenotypes, including COVID-19 positive and recovered. Microclots with varying structure and composition were detected in plasma samples from all the COVID-19 patients, regardless of symptom severity. Microclots were classified based on their composition as microclot composites, fibrin-rich microclots, or platelet aggregates. To understand whether microclot structure and composition would differ between COVID-19 subphenotypes, we quantified the overall size distribution and prevalence of microclot subtypes in plasma from COVID-19 compared to healthy donors. Our findings highlight that label-free high-throughput microscopy can be used as a point-of-care technique to visualize and quantify the presence of microclots directly in plasma without the need for complicated sample preparation techniques. Knowledge gained from such microclot analytics could be useful for developing effective treatment strategies to prevent and manage thrombotic complications in COVID-19 and long COVID patients, thereby improving patient outcomes.

RESULTS AND DISCUSSION

Label-Free Digital Holo-Tomographic Microscopy of Synthetically Prepared Blood Clots

Previously, we have shown that DHTM can be used to visualize and quantify the morphometry of red blood cells as they interact with ibuprofen drugs in a non-invasive and label-free manner, with high spatial resolution.[37] In this study, we first extended the use of DHTM (Figure S1) to resolve the structure and composition of synthetically prepared blood clot fragments in an aqueous solution (Figure 1). Blood from a healthy and a convalescent COVID-19 donor was collected and allowed to clot before imaging with DHTM (Methods). Details on the demographic information on the donors are provided in Table S1. Figure 1A shows the 3D refractive index (RI) tomogram of synthetically prepared blood clot fragments from a healthy donor, revealing differences in the structural composition based on variations in RI values. From the corresponding segmented RI tomogram (Figure 1B), micrometer-sized blood clot fragments were digitally stained based on the RI values (Figure 1C), and a color-coded label was assigned to discriminate between different structural components, including fibrin strands and non-fibrin structures. The same RI classification was applied to spatially well-resolved blood clot fragments obtained from a COVID-19 donor (Figure 1D), revealing similar structural components depicting a net-like fibrin network with smaller and circular non-fibrin structures.

To further understand the compositional differences within a micrometer-size blood clot structure, we performed Raman spectroscopy on the same samples (Methods) used previously for DHTM measurements based on which data shown in Figure 1A,D were obtained. Figure 1E shows the Raman spectra collected from synthetically prepared blood clot fragments of healthy (black spectrum) and COVID-19 (red spectrum) donors. Spectrochemical analysis revealed the presence of signal peaks in the spectral regions associated with the presence of fibrin (976, 1248, and 1342 cm^{-1}),[38] hemoglobin (567, 1000, 1368, 1542, and 1575 cm^{-1}),[38,39] and lipids (1266, 1300, 1444, and 1655 cm^{-1}).[40] The averaged spectral signature of blood clot fragments from a donor with COVID-19 presented spectral similarities to that of healthy blood clots in the hemoglobin and lipid regions. In the hemoglobin region, an increase in the intensity of the peak at 561 cm^{-1} was detected in the COVID-19 blood clots, indicative of stretching of the Fe−O_2 bond.[39] In contrast, a decrease in the intensity of the peak at 1360 cm^{-1} was observed in COVID-19 blood clots compared with the healthy blood clots. In the lipid regions, a decrease in the intensity of the peaks at 1266 and 1655 cm^{-1} as well as the peaks at 1305 and 1450 cm^{-1} was detected in the COVID-19 blood clot samples. These peaks are associated with unsaturated and saturated lipids, respectively.[40] In the fibrin regions, a maximum peak at 976 cm^{-1} was detected in the COVID-19 samples but not in the healthy blood clot fragments. Here, the presence of a peak at 937 cm^{-1} may be indicative of a shift of the fibrin band in healthy blood clots. In contrast, both blood clot samples presented a maximum peak in a secondary fibrin region at 1342 cm^{-1}, with a lower signal intensity in the COVID-19 blood clot fragments. The peak at 1100 cm^{-1} observed only in the blood clot fragments from a donor with COVID-19 has been previously reported to stem either from ghost RBCs or from heme present in biological samples.[38−40]

https://doi.org/10.1021/cbmi.3c00126
Chem. Biomed. Imaging XXXX, XXX, XXX−XXX

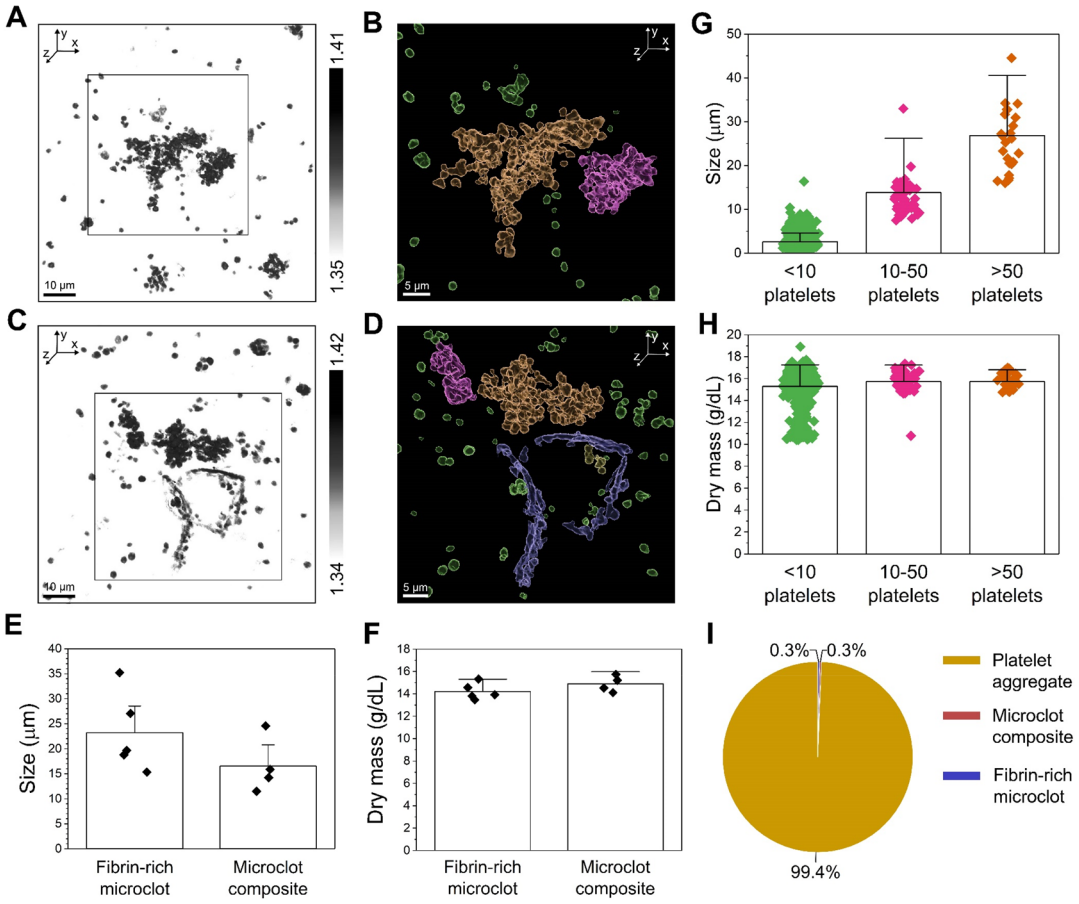

Figure 2. Structural analysis of microclots in plasma of a COVID-19 positive patient with mild symptomatology (PLS-CVDP2). (A) Refractive index (RI) tomogram of platelet aggregates in plasma. (B) Corresponding segmented RI tomogram of the platelet aggregates of different sizes from the inset in (A). (C) RI tomogram of a fibrin-rich microclot and platelet aggregates in plasma. (D) Corresponding segmented RI tomogram of the fibrin-rich microclot and the platelet aggregates of different sizes from the inset in (C). (E, F) Size and dry mass of fibrin-rich microclots and microclot composite structures in plasma. (G, H) Size and dry mass of platelet aggregates in plasma. Error bars represent the standard deviation from the mean. (I) Pie chart showing the microclot composition in plasma of donor PLS-CVDP2.

Such differences in the spectra between the healthy and the COVID-19 blood clot samples may be indicative of changes occurring in the overall structure and composition of blood clots. The Raman spectroscopy data presented here are based on a combined average of several blood clot fragments distributed across the surface.

The structural parameters of healthy and COVID-19 blood clot fragments were extracted and quantified including the overall size, the fibrin fibril diameter, and the dry mass. A two-sample t test revealed a significant increase in clot length (healthy: 50.1 ± 18.9 μm; COVID-19: 66.2 ± 21.5 μm) (Figure 1F) and width (healthy: 31.0 ± 14.5 μm; COVID-19: 49.1 ± 19.8 μm) (Figure 1G) in COVID-19 compared to healthy blood clots, suggesting an overall difference in the size of the clot fragments. In addition, the diameter of the fibrin fibrils was significantly larger in the COVID-19 samples compared to the healthy samples (healthy: 0.64 ± 0.13 μm; COVID-19: 0.77 ± 0.14 μm; Figure 1H). Finally, the dry mass was obtained from the RI measurements (Methods). No significant difference was detected between the healthy (5.90 ± 1.57 g/dL) and the COVID-19 (5.26 ± 1.5 g/dL) samples (Figure 1I), indicating a comparable structural composition of the analyzed blood clot fragments.

Structural Analysis of Microclots in COVID-19 Plasma

The described DHTM imaging and analysis protocol was employed to assess the presence of microclots in the plasma of five patients with COVID-19 (Table S2). Different COVID-19 subphenotypes were identified, depending on the presence (positive or recovered) and severity of symptoms (mild, moderate, asymptomatic) at the time of blood collection. Microclots of varying sizes were observed during DHTM measurements in plasma from all five patients. The detected microclots were classified based on their composition: (i) microclot composites, defined as micrometer-size clot structures with mixed composition of plasma proteins;[34] (ii) fibrin−rich microclots, defined as micrometer-size clot structures with prevalent fibrin fibrils; (iii) platelet aggregates, defined as aggregated platelets of different sizes depending on the number of platelets (<10 platelets, 10−50 platelets, and >50 platelets). Microclots were found in all the analyzed COVID-19 plasma samples, regardless of age, symptomatology, and IgG and IgM antibody levels. Figure 2 shows the results of the DHTM-based analysis of plasma collected from a 27-year-old female, COVID-19 positive patient (donor identified as sample PLS-CVDP2) with a mild symptomatology subphenotype (Methods). The 3D RI tomograms show highly aggregated platelets and the presence of a fibrin-rich microclot of moderate size (~35 μm; Figure 2A,C). The

https://doi.org/10.1021/cbmi.3c00126
Chem. Biomed. Imaging XXXX, XXX, XXX−XXX

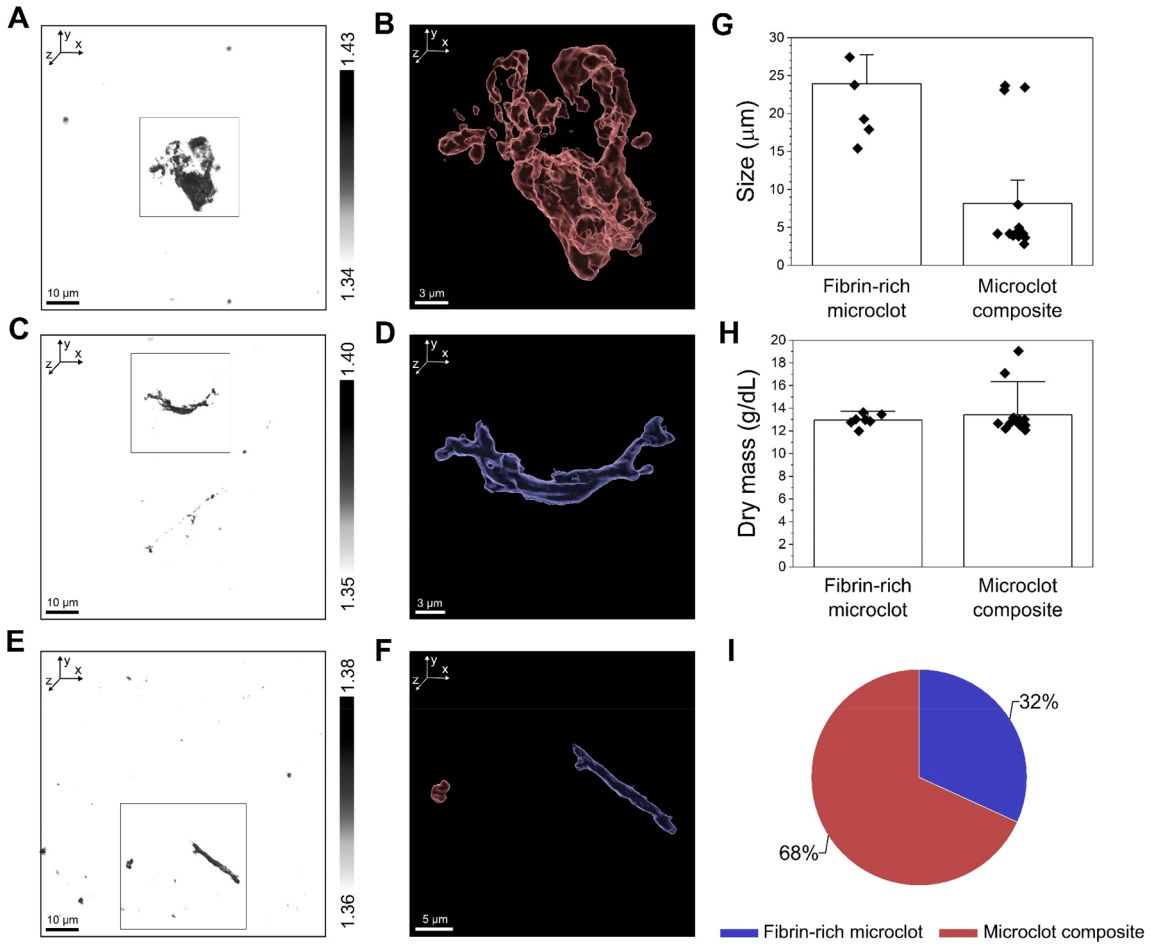

Figure 3. Structural analysis of microclots in plasma of a COVID-19 positive patient with moderate symptomatology (PLS-CVDP1). (A) Refractive index (RI) tomogram of a microclot composite in plasma. (B) Corresponding segmented RI tomogram of the microclot composite from the inset in (A). (C) RI tomogram of a fibrin-rich microclot in plasma. (D) Corresponding segmented RI tomogram of the fibrin-rich microclot from the inset in (C). (E) RI tomogram of a microclot composite and fibrin-rich microclots in plasma. (F) Corresponding segmented RI tomogram of a microclot composite and the fibrin-rich microclot from the inset in (E). (G, H) Size and dry mass of fibrin-rich microclots and microclot composite structures in plasma. Error bars represent the standard deviation from the mean. (I) Pie chart showing the microclot composition in plasma of donor PLS-CVDP1.

microclot structures were segmented and classified based on the microclot type and platelet aggregate size (Figure 2B,D). To morphologically characterize the microclots, the size and the dry mass were extracted and quantified from the RI tomograms (Methods). Fibrin-rich microclots were bigger (mean = 23.2 ± 7.9 μm) than microclot composites (mean = 16.5 ± 5.6 μm), likely due to the length of the fibrin strands in a network format (Figure 2E). In contrast, the dry mass did not differ between the microclot structures (fibrin-rich microclots = 14.2 ± 0.7 g/dL; microclot composite = 14.9 ± 0.7 g/dL; Figure 2F). The size of platelet aggregates differed markedly based on the number of platelets (<10 platelets = 2.6 ± 1.3 μm, 10−50 platelets = 13.8 ± 8.2 μm, >50 platelets = 26.8 ± 9.1 μm), with platelet aggregates of >50 platelets reaching sizes of up to 45 μm (Figure 2G). No major differences were observed in the dry mass of the platelet aggregates (<10 platelets = 15.3 ± 1.3 g/dL, 10−50 platelets = 15.7 ± 1.0 g/dL, >50 platelets = 15.7 ± 0.7 g/dL) (Figure 2H), likely because these microclot structures are composed of mostly platelets. A total of ∼4 microclot composite structures, ∼5 fibrin-rich microclots, and ∼1570 platelet aggregates were observed in 75 μL of plasma (Figure 2I), indicating extensive platelet pathology characterized by aggregated platelets in plasma from donor PLS-CVDP2.

Next, we analyzed the plasma of a 26-year-old female, COVID-19 positive patient (donor identified as sample PLS-CVDP1) with a moderate symptomatology subphenotype (Figure 3 and Methods). A total of ∼20 microclots were detected in 75 μL of plasma, classified as either a microclot composite (Figure 3A) or fibrin-rich microclots (Figure 3C,E). The segmented and classified 3D RI tomograms show the spatially magnified structure of a microclot composite (Figure 3B) and reveal the presence of single fibrin fibrils in the plasma of this individual (Figure 3D,F). A clear size difference was observed between the two types of microclot structures (Figure 3G). Similar to PLS-CVDP2, the measured fibrin-rich microclots appeared larger (mean = 24.0 ± 6.7 μm) compared to the microclot composites (mean = 8.1 ± 8.0 μm). Interestingly, the dry mass did not differ between microclot structures (fibrin-rich microclots = 12.9 ± 0.5 g/dL, microclot composite = 13.4 ± 1.9 g/dL), except two microclot composites (Figure 3H). Overall, the described COVID-19 subphenotype was characterized by prevalent microclot composite structures and a few fibrin-rich microclots (Figure

https://doi.org/10.1021/cbmi.3c00126
Chem. Biomed. Imaging XXXX, XXX, XXX−XXX

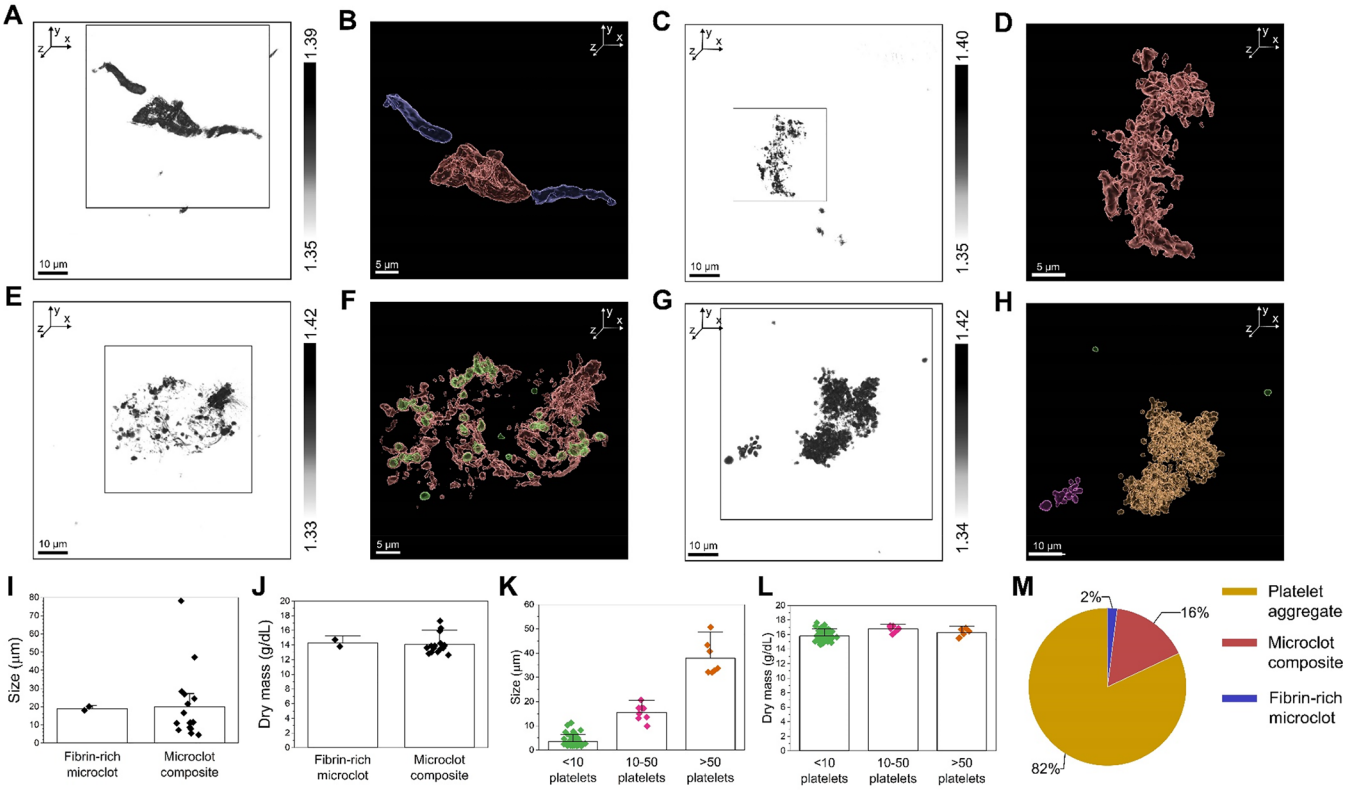

Figure 4. Structural analysis of microclots in plasma of a COVID-19 recovered patient with mild symptomatology (PLS-CVDR2). (A) Refractive index (RI) tomogram of a microclot composite and fibrin-rich microclots in plasma. (B) Corresponding segmented RI tomogram of the microclot composite and fibrin-rich microclots from the inset in (A). (C) RI tomogram of a microclot composite in plasma. (D) Corresponding segmented RI tomogram of the microclot composite from the inset in (C). (E) RI tomogram of a microclot composite with platelet aggregates in plasma. (F) Corresponding segmented RI tomogram of the microclot composite with platelet aggregates from the inset in (E). (G) RI tomogram of platelet aggregates in plasma. (H) Corresponding segmented RI tomogram of the platelet aggregates of different sizes from the inset in (G). (I, J) Size and dry mass of fibrin-rich microclots and microclot composite structures in plasma. (K, L) Size and dry mass of platelet aggregates in plasma. Error bars represent the standard deviation from the mean. (M) Pie chart showing the microclot composition in plasma of donor PLS-CVDR2.

3I). Platelet clumping was not observed in plasma from the donor PLS-CVDP1.

Finally, we report the analysis of plasma collected from a 23-year-old female, COVID-19 recovered patient (donor identified as sample PLS-CVDR2) with mild symptomatology subphenotype (Figure 4 and Methods). The presence of microclots was detected in 75 μL of plasma, despite this patient being classified as having recovered COVID-19 and no longer experiencing symptoms at the time of blood collection. Microclot composites (n = 16) presented varying morphologies, including more dense structures with fibrin fibrils (Figure 4A,B) and net-like structures intertwined with platelets (Figure 4C−F). Platelet clumping was also observed (n = 83) (Figure 4G,H). The size of fibrin-rich microclots and microclot composites did not significantly differ (fibrin-rich microclots = 19.0 ± 1.6 μm, microclot composites = 20.1 ± 19.1 μm), as shown in Figure 4I. However, a few large microclot composite structures were detected, measuring up to ∼80 μm in size. Similarly, the dry mass was consistent between the microclot structures (fibrin-rich microclots = 14.3 ± 0.6 g/dL, microclot composite = 14.1 ± 1.3 g/dL) (Figure 4J). Platelet aggregates varied in size depending on the number of platelets (<10 platelets = 3.5 ± 1.9 μm, 10−50 platelets = 15.5 ± 3.3 μm, >50 platelets = 37.9 ± 7.2 μm), reaching sizes of up to ∼50 μm (Figure 4K). Instead, the dry mass did not differ between platelet aggregate structures (<10 platelets = 15.8 ± 0.6 g/dL, 10−50 platelets = 16.8 ± 0.4 g/dL, >50 platelets = 16.3 ± 0.6 g/dL) (Figure 4L). Overall, this diverse COVID-19 subphenotype presented a mixed composition of microclot structures with platelet clumping representing the most prevalent feature (Figure 4M). The structural analysis of the remaining COVID-19 subphenotypes, including a COVID-19 positive female patient with no symptomatology (PLS-CVDP3) and a COVID-19 recovered female patient with moderate symptomatology (PLS-CVDR1), and of the healthy controls are provided in Figures S2, S3, and S4, respectively. Interestingly, microclots were detected in plasma from the donor identified as PLS-CVDP3 even in the absence of clinical features (Figure S2).

Quantification of Microclot Structure and Composition in COVID-19 Subphenotypes

Following the in-depth description of the DHTM analysis of plasma from single COVID-19 patients, we present the results on the quantification of microclot structure and composition of all COVID-19 subphenotypes as well as five healthy controls (Figure 5). Figure 5A shows the prevalence of fibrin-rich microclots and microclot composites in 75 μL of plasma from five healthy donors and five patients with different COVID-19 subphenotypes. Overall, these microclot structures were more prevalent in plasma from all COVID-19 samples compared to the healthy controls (fibrin-rich microclot: 1 ± 2; microclot composite: 2 ± 2). Within the COVID-19 samples, microclot composites were more prevalent compared to with fibrin-rich

https://doi.org/10.1021/cbmi.3c00126
Chem. Biomed. Imaging XXXX, XXX, XXX−XXX

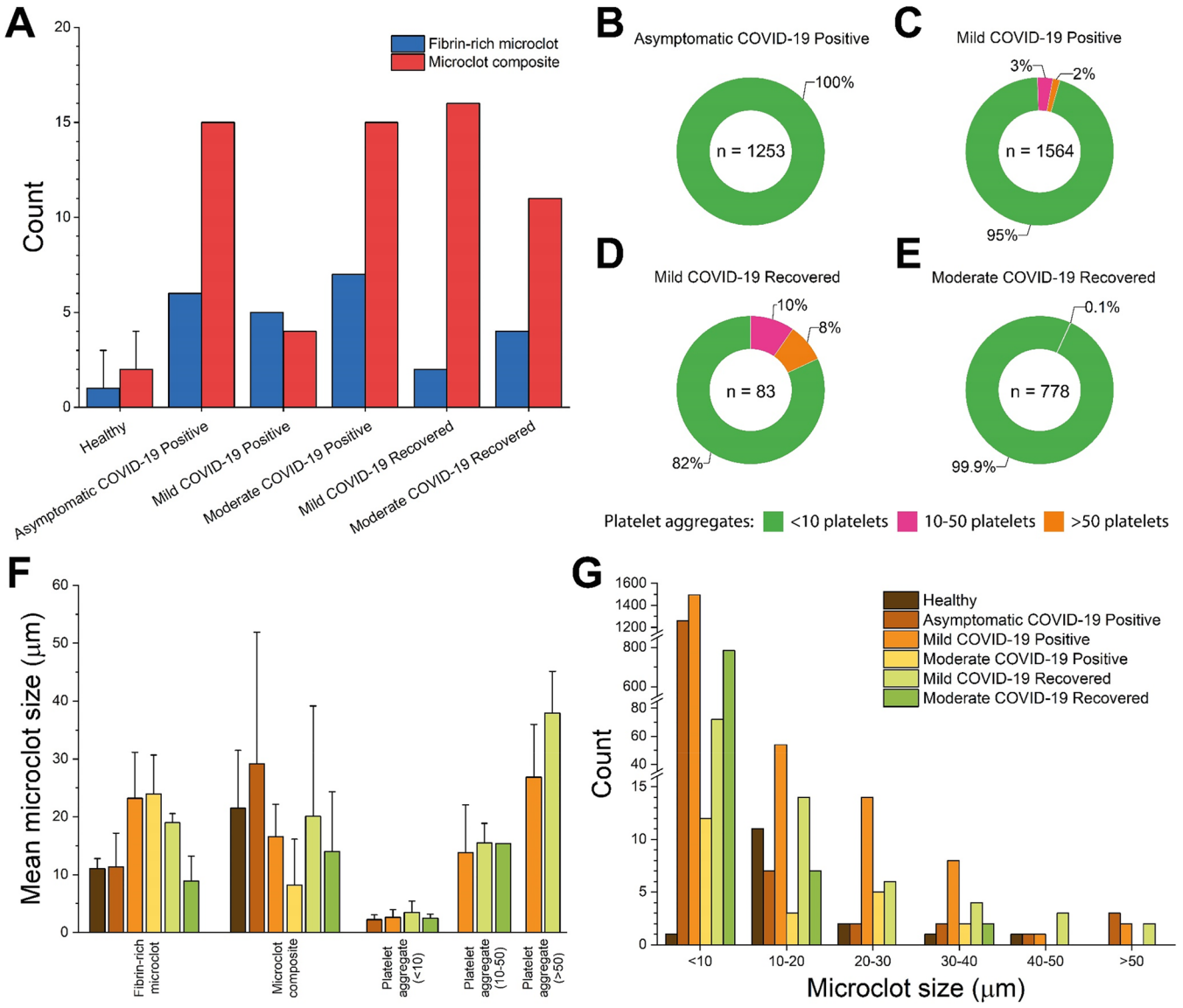

Figure 5. Morphological characterization of microclots in healthy and COVID-19 positive and recovered patients. (A) Prevalence of fibrin-rich microclots and microclot composites detected in 75 μL of plasma from healthy and COVID-19 positive and recovered patients. (B) Prevalence of platelet aggregates detected in 75 μL of plasma from a COVID-19 positive patient with no symptomatology, (C) a COVID-19 positive patient with mild symptomatology, (D) a COVID-19 recovered patient with mild symptomatology, and (E) a COVID-19 recovered patient with moderate symptomatology. (F) Mean microclot size plotted against the microclot type and grouped by healthy and COVID-19 subphenotypes. Error bars correspond to the standard deviation. (G) Prevalence of microclots plotted against the microclot size and grouped by healthy and COVID-19 subphenotypes.

microclots, except for the COVID-19 positive patient with mild symptomatology, which presented an equal number of microclot structures (Figure 5A). Additionally, a trend for a higher prevalence of fibrin-rich microclots in COVID-19 positive patients compared to that in COVID-19 recovered patients can be observed (Figure 5A). Platelet clumping was also more prevalent in the COVID-19 positive patients compared to the recovered subphenotypes, although it was not observed in the COVID-19 positive patient with moderate symptomatology (Figure 5B–E). Aggregated platelets were not detected in any of the healthy samples. In all samples where platelet clumping was detected, platelet aggregates of <10 platelets were mostly prevalent (Figure 5B–E). Interestingly, larger platelet aggregates composed of >10 platelets were detected in the plasma of both COVID-19 patients (positive and recovered) with mild symptomatology (Figure 5B–E). However, a correlation between microclot type and prevalence with the analyzed COVID-19 subphenotypes could not be determined.

Due to the importance of microclot size in the risk of occlusion of microcapillaries, the mean microclot size was plotted against the microclot type and grouped by healthy and COVID-19 subphenotypes (Figure 5F). The size of the detected microclots was averaged between 1 and 60 μm. Size variation within fibrin-rich microclots and microclot composites between plasma samples was likely dependent on the length of the fibrin fibrils and on the mixed composition of the microclot composites, respectively (Figure 5F). The average size of platelet aggregates was comparable between the COVID-19 subphenotypes and depended on the number of platelets in each aggregate (Figure 5F). The prevalence of microclots was also plotted against the microclot size and

https://doi.org/10.1021/cbmi.3c00126
Chem. Biomed. Imaging XXXX, XXX, XXX−XXX

grouped by healthy and COVID-19 subphenotypes (Figure 5G). For all of the COVID-19 subphenotypes, microclots were mostly prevalent in the size range between 1 and 10 μm. Overall, the severity of the COVID-19 symptomatology as well as the positive or recovered subphenotype did not seem to correlate with the size of the measured microclots. Moreover, a correlation between microclot prevalence and size and the patient age as well as the IgG and IgM antibody levels was not observed (Figures S5 and S6) within the limited number of patient samples analyzed in the present study.

CONCLUSION

Microclots continue to receive clinical research interest as potential indicators of long COVID.[1,3−5,8,9,12,15,20,26,36] In this study, we employed DHTM as an analytical tool to characterize the composition of plasma from patients with COVID-19 subphenotypes. To test our imaging and analysis protocol, we studied synthetically prepared fixed blood clot fragments in an aqueous solution using DHTM. The preliminary step was to identify and obtain the quantitative morphological parameters from 3D RI tomograms of the synthetically prepared blood clot fragments. Blood clot structure can be described by parameters such as the fibrin fibril diameter, fibrin length, clot composition, clot density, and clot porosity.[41] These physical parameters also provide deeper insights into clot stiffness, stability, and degradation dynamics, which play a crucial role in hemostasis.[30,41,42] Significant size differences were observed between healthy and COVID-19 blood clot fragments with regard to the size and fibrin fibril thickness. Although these blood clots were passed through a 30 μm filter to fragment them, in general, larger fragments, evidenced by thicker fibrin fibrils, derived from COVID-19 patients, are suggestive of increased clot rigidity. Clot composition and density, estimated from the dry mass, were similar between the two samples, also supported by the spectrochemical signature from the Raman measurements. Importantly, digital staining revealed details of an intricate network of fibrin fibrils with smaller and more circular structures trapped between the fibrils. Similar to fluorescent markers in immunofluorescence, digital staining allows for specific labeling of multiple structures based on the refractive index values but without altering the inherent features of the sample.[43] Although we were able to demonstrate the structural characterization of fixed blood clot fragments in an aqueous solution, we cannot explicitly identify the non-fibrin structures observed within these clot fragments. This is due to the inability to access the spatial RI distribution of protein and cellular structures smaller than the DHTM lateral resolution (~200 nm). Combining complementary techniques, such as fluorescent-based labeling or expansion microscopy with DHTM could be used to elucidate the nature of the non-fibrin structures.[44] Taken together, the DHTM analysis of micrometer-sized blood clot fragments reveals remarkable details of clot structure and composition in a label-free manner, which can be quantified and further classified into different blood clot types. The morphological parameters that we identified in the first part of our study were then further extended to directly characterize microclots in plasma.

Next, we extended our DHTM-based imaging protocol to study the composition of plasma from patients with COVID-19 and healthy donors. Similar to previous studies,[4,9,20,23,26,36] we observed microclots in all COVID-19 plasma samples. However, only a few microclots were detected in plasma from healthy donors, suggesting that microclotting is a salient feature of COVID-19. One of the most notable findings is the structural diversity of the observed microclots, which we have further classified based on their composition: microclot composites, fibrin-rich microclots, and platelet aggregates. Microclot composites were found in all COVID-19 plasma samples, with the highest prevalence in the COVID-19 positive patient with moderate symptomatology. These composites structurally resemble the microclots previously reported by Pretorius and colleagues using fluorescence microscopy,[4,9,26,36] with a likely mixed composition of fibrin and other proteins.[3,5,34] In some cases, platelets appear to be trapped between the microclot composite structures. The structural variation in microclot composites observed throughout the COVID-19 plasma samples evidence the presence of a mixed population of fibrin structures and proteins. Microclots were also detected in the form of long fibrin networks. Single fibrin fibrils were also observed, which may stem from clot degradation and fibrinolysis.[4,20,29,42] Consistent with previous studies,[4,9,36] platelet activation and persistent platelet clumping were prevalent features of platelet pathology in all COVID-19 plasma samples, except for the COVID-19 positive patient with moderate symptomatology. Interestingly, the plasma of this patient was characterized by microclot composites and fibrin-rich microclots only, albeit presenting the most severe clinical presentation and high levels of IgG antibodies. Importantly, the size of the measured microclots in COVID-19 plasma samples using DHTM could be of potential clinical interest regarding their ability to occlude microvasculature and thus impede oxygen transport.[5] Microclots formed in the vascular system are likely to explain the heterogeneous symptomatology and multiorgan dysfunction observed in COVID-19 and long COVID patients.[14,45]

Based on our DHTM analysis, a correlation between microclot type, size, and prevalence and COVID-19 subphenotypes could not be established in the small analyzed cohort. However, it is possible that many more pre-existing individual risk factors, aside from SARS-CoV-2 infection status (COVID-19 positive or recovered) and symptomatology, may contribute to the presence and the extent of COVID-19-related microvascular injury, including a history of smoking, vitamin D deficiency, exposure to air pollutants, and the presence of other pathologies such as cancer or diabetes mellitus, for which we could not account for in our study.[1,5,6,26] The identification of comorbidities is particularly relevant in assessing an individual's risk of developing long COVID.[9,16,18] It is important to note that the symptomatology reported for the analyzed cohort (e.g., headache, fever) may not directly reflect the coagulopathy status of the patients upon SARS-CoV-2 infection, which in turn would explain why we did not observe a distinct correlation between microclot prevalence and size with COVID-19 subphenotypes. The role of potential risk factors associated with the presence of microclots and the wide spectrum of clinical manifestations of both acute and long COVID may only be unraveled with a larger cohort.[46] Future studies aimed at validating our DHTM methodology will require a larger sample size to be analyzed, comprising patients suffering from both acute COVID-19 and long COVID conditions. Sample stratification also needs to be included in the study for the identification of different comorbidities and risk factors as well as differentiation between SARS-CoV-2 variants.

https://doi.org/10.1021/cbmi.3c00126
Chem. Biomed. Imaging XXXX, XXX, XXX−XXX

In conclusion, the label-free DHTM-based approach demonstrated in our study could serve as a powerful tool for screening microclots in plasma. Information obtained in a label-free manner from such an approach, with high spatial resolution, could provide deeper insights into understanding the role of microclots in health and disease. Furthermore, the approach described in this paper not only is limited to microclot analysis in plasma but also can be extended to resolve micrometer-size protein fibrils implicated in neurocognitive disorders in cerebrospinal fluid.[47] We anticipate that such an analytical technique, compatible with operation under standard laboratory conditions, could be easily integrated with the existing clinical pipeline for digitally monitoring protein aggregates in body fluids and assessing disease stages.

METHODS

Patient Characteristics

In this study, we present data from healthy individuals, COVID-19 positive patients, and patients who recently recovered from a coronavirus 2 (SARS-CoV-2) infection upon blood collection. The patient characteristics were determined by in-house clinicians at the commercial source from which the samples were purchased. Fixed blood clot fragments in aqueous solution were prepared from fresh human blood collected from one healthy donor and one COVID-19 convalescent donor in the United States (Zenbio). In contrast, plasma was collected from five healthy donors in the United Kingdom (BioIVT) and five adult COVID-19 convalescent donors in the United States (BioIVT). Three COVID-19 patients were classified as COVID positive as they tested positive for the SARS-coV-2 serology test (IgG/IgM positive, IgG positive/IgM negative), and they were symptomatic at the time of blood collection. Blood samples were collected within one month from the diagnosis of SARS-CoV-2 infection. In contrast, two COVID-19 patients were classified as having recovered COVID as they were no longer symptomatic at the time of blood collection and presented with either a positive or negative serology test (IgG positive/IgM negative and IgG/IgM negative). Blood samples were collected between two and three months after COVID-19 diagnosis. The type and severity of symptoms in the COVID-19 patients were heterogeneous. Within the COVID positive donor group, one was asymptomatic, one presented mild symptoms (body or muscle aches, chills, and headache), and one had moderate symptoms (body or muscle aches, chest pain, chills, confusion, congestion, cough, diarrhea, fatigue, headache, loss of smell, runny nose, shortness of breath, sneezing, trouble breathing, and weakness). Similarly, in the COVID recovered subgroup, one donor had experienced mild symptoms (fatigue, headache, loss of smell and taste) and one donor had experienced a more moderate symptomatology (body or muscle aches, cough, diarrhea, fatigue, fever, headache, loss of smell and taste, and shortness of breath). Summaries of the demographics and SARS-CoV-2 serology test results are presented in Table S2.

Preparation of Fixed Blood Clot Samples

Healthy and COVID-19 fixed blood clot samples were commercially obtained (ZenBio) from a single donor, respectively. Whole blood was collected via venipuncture, added to an empty tube, and allowed to clot. The clot was mechanically disrupted and passed through a 30 μm filter to generate smaller clot fragments. Finally, the clots were fixed in 4% paraformaldehyde (PFA), and they were provided as 1 mL aliquots and stored at 4 °C. For DHTM imaging, 200 μL of blood clots in aqueous solution was transferred to a 35 mm Ibidi ibiTreat μ-Dish (Ibidi GmbH, Germany).

Preparation of Plasma

Plasma was commercially obtained (BioIVT) for healthy and convalescent patients with COVID-19 patients. Whole blood was collected in K2EDTA vacutainers and centrifuged to separate the plasma from the cell pellet. Plasma samples were transported and stored at −20 °C. For all plasma samples, 50 μL of plasma was diluted in 200 μL of Alsever's solution (Sigma-Aldrich, A3551) and 250 μL was transferred to a 35 mm Ibidi ibiTreat μ-Dish (Ibidi GmbH, Germany) for DHTM imaging.

Label-Free Digital Holo-tomographic Microscopy

Label-free holo-tomographic imaging was performed using a 3D Cell Explorer microscope (Nanolive SA, Switzerland). Before each measurement, the Petri dish containing either the fixed blood clots in aqueous solution or the plasma solution was placed in the microscope sample holder, and blood clots were allowed to sediment to the bottom of the Petri dish for 10 min before imaging. A total of 75 μL of plasma was analyzed for each patient. Each image acquired with the digital holo-tomographic microscope corresponds to a field of view of 90 μm × 90 μm × 30 μm. DHTM was operated under standard laboratory conditions.

Image Processing and Analysis

3D RI stacks obtained by DHTM were exported as TIFF files and imported into the open-source software Tomviz for 3D RI visualization. For the visualization of clot-specific structures, 3D stacks obtained by DHTM were digitally stained based on the RI values using STEVE (Nanolive SA, Switzerland), and each channel was exported in the form of a 3D stack as a TIFF file. The single-channel 3D stacks were imported into the open-source software Fiji, and a 2 × 2 × 2 mean filter was applied as a noise removal filter. The single channels were merged into one image, exported as a TIFF file, and imported into Imaris 9.8 (Bitplane AG, Switzerland) to achieve 3D surface segmentation. First, stacks were cropped along the x-axis and y-axis to exclude potential signal noise artifacts from the imaging process. Next, a surface was fitted for each channel with absolute intensity and automatic thresholding to achieve an accurate signal segmentation. For the structural analysis and quantification of the blood clots, 3D RI stacks obtained by DHTM were imported into Imaris 9.8 and were cropped along the x-axis and y-axis to exclude potential signal noise artifacts. A 3 × 3 × 3 median filter was applied as a noise removal filter, and a surface was fitted with absolute intensity and automatic thresholding. The morphologically relevant features were quantitatively measured, including the clot length, width, surface area, volume, and mean RI (Table S3). The dry mass was calculated from the mean RI value of each blood clot, obtained from the 3D RI tomograms, using the following formula:[48]

$$\text{dry mass} = \left(\frac{n_{\text{clot}}}{n_{\text{H}_2\text{O}}} - 1\right) \times \frac{1}{\alpha}$$

where n_{clot} is the mean RI value of the blood clot, n_{H2O} is the RI of water (1.333), and α is the wavelength-dependent RI increment, which was set to 0.001983 for λ = 520 nm.[49] Approximately a 2 h time period is required per sample to perform the sample preparation, image analysis, and quantification.

Raman Spectroscopy Setup and Measurements

Raman spectra were obtained using an NT-MDT NTEGRA Spectra system equipped with an Olympus LMPLFLN 100× objective with numerical aperture (NA) of 0.8 and spectrometer grating of 600 g/mm. Samples were illuminated with a 561 nm wavelength laser (10 mW laser power at the sample). Spectra were acquired in the reflection mode with an integration time of 20 s and 10 accumulations. To obtain a representative spectrum of the measured sample, multiple spectra were acquired at different locations of the sample and then averaged. Raman spectroscopy was conducted only on air-dried fixed blood clots in an aqueous solution deposited on SuperFrost glass slides.

ASSOCIATED CONTENT

Data Availability Statement

All data needed to evaluate the conclusions in the paper are present in the paper and/or the Supporting Information.

https://doi.org/10.1021/cbmi.3c00126
Chem. Biomed. Imaging XXXX, XXX, XXX−XXX

Additional data related to this paper may be requested from the authors.

Supporting Information

The Supporting Information is available free of charge at https://pubs.acs.org/doi/10.1021/cbmi.3c00126.

Summary of the sample demographics and supplementary figures of DHTM on COVID-19 and healthy plasma (PDF)

AUTHOR INFORMATION

Corresponding Author

Peter Niraj Nirmalraj − *Transport at Nanoscale Interfaces Laboratory, Swiss Federal Laboratories for Materials Science and Technology, Dübendorf CH-8600, Switzerland;* orcid.org/0000-0002-2282-6781; Email: peter.nirmalraj@empa.ch

Authors

Talia Bergaglio − *Transport at Nanoscale Interfaces Laboratory, Swiss Federal Laboratories for Materials Science and Technology, Dübendorf CH-8600, Switzerland; Graduate School for Cellular and Biomedical Sciences, University of Bern, Bern CH-3012, Switzerland*

Olena Synhaivska − *Transport at Nanoscale Interfaces Laboratory, Swiss Federal Laboratories for Materials Science and Technology, Dübendorf CH-8600, Switzerland*

Complete contact information is available at: https://pubs.acs.org/10.1021/cbmi.3c00126

Author Contributions

T.B. and P.N.N. planned the study. T.B. conducted the holotomographic measurements, image processing, and data analysis. O.S. conducted the Raman spectroscopy measurements and data analysis. P.N.N. supervised the study. T.B. and P.N.N. wrote the manuscript. All authors discussed the results and commented on the manuscript.

Notes

The authors declare no competing financial interest.

ACKNOWLEDGMENTS

T.B. and P.N.N. thank Alex Dommann for strategic support and Susanne Wegener for useful discussions. This paper benefited from discussions at the Synapsis Foundation Dementia Research Workshop in November 2023. This work used the computational resources provided by the University of Bern, Switzerland. T.B. thanks Guillaume Witz at the Microscopy Imaging Center at the University of Bern for technical assistance.

REFERENCES

(1) Leng, A.; Shah, M.; Ahmad, S. A.; Premraj, L.; Wildi, K.; Li Bassi, G.; Pardo, C. A.; Choi, A.; Cho, S.-M. Pathogenesis Underlying Neurological Manifestations of Long COVID Syndrome and Potential Therapeutics. *Cells* **2023**, *12* (5), 816.

(2) Gupta, A.; Madhavan, M. V.; Sehgal, K.; Nair, N.; Mahajan, S.; Sehrawat, T. S.; Bikdeli, B.; Ahluwalia, N.; Ausiello, J. C.; Wan, E. Y.; et al. Extrapulmonary manifestations of COVID-19. *Nature Medicine* **2020**, *26* (7), 1017−1032.

(3) Grobler, C.; Maphumulo, S. C.; Grobbelaar, L. M.; Bredenkamp, J. C.; Laubscher, G. J.; Lourens, P. J.; Steenkamp, J.; Kell, D. B.; Pretorius, E. Covid-19: The Rollercoaster of Fibrin(Ogen), D-Dimer, Von Willebrand Factor, P-Selectin and Their Interactions with Endothelial Cells, Platelets and Erythrocytes. *International Journal of Molecular Sciences* **2020**, *21* (14), 5168.

(4) Pretorius, E.; Vlok, M.; Venter, C.; Bezuidenhout, J. A.; Laubscher, G. J.; Steenkamp, J.; Kell, D. B. Persistent clotting protein pathology in Long COVID/Post-Acute Sequelae of COVID-19 (PASC) is accompanied by increased levels of antiplasmin. *Cardiovascular Diabetology* **2021**, *20* (1), 172.

(5) Kell, D. B.; Laubscher, G. J.; Pretorius, E. A central role for amyloid fibrin microclots in long COVID/PASC: origins and therapeutic implications. *Biochem. J.* **2022**, *479* (4), 537−559.

(6) Bikdeli, B.; Madhavan, M. V.; Jimenez, D.; Chuich, T.; Dreyfus, I.; Driggin, E.; Nigoghossian, C.; Ageno, W.; Madjid, M.; Guo, Y.; et al. COVID-19 and Thrombotic or Thromboembolic Disease: Implications for Prevention, Antithrombotic Therapy, and Follow-Up: JACC State-of-the-Art Review. *J. Am. Coll Cardiol* **2020**, *75* (23), 2950−2973.

(7) Rahi, M. S.; Jindal, V.; Reyes, S.-P.; Gunasekaran, K.; Gupta, R.; Jaiyesimi, I. Hematologic disorders associated with COVID-19: a review. *Annals of Hematology* **2021**, *100* (2), 309−320.

(8) Monje, M.; Iwasaki, A. The neurobiology of long COVID. *Neuron* **2022**, *110* (21), 3484−3496.

(9) Pretorius, E.; Venter, C.; Laubscher, G. J.; Kotze, M. J.; Oladejo, S. O.; Watson, L. R.; Rajaratnam, K.; Watson, B. W.; Kell, D. B. Prevalence of symptoms, comorbidities, fibrin amyloid microclots and platelet pathology in individuals with Long COVID/Post-Acute Sequelae of COVID-19 (PASC). *Cardiovasc Diabetol* **2022**, *21* (1), No. 148.

(10) Schiavone, B.; Dore, G. J.; Stone, E.; Matthews, G. V.; Darley, D. R. An update on long COVID and its management. *Medicine Today* **2023**, *24*, 37−43.

(11) Scholkmann, F.; May, C. A. COVID-19, post-acute COVID-19 syndrome (PACS, "long COVID") and post-COVID-19 vaccination syndrome (PCVS, "post-COVIDvac-syndrome"): Similarities and differences. *Pathol Res. Pract* **2023**, *246*, No. 154497.

(12) Nalbandian, A.; Sehgal, K.; Gupta, A.; Madhavan, M. V.; McGroder, C.; Stevens, J. S.; Cook, J. R.; Nordvig, A. S.; Shalev, D.; Sehrawat, T. S.; et al. Post-acute COVID-19 syndrome. *Nature Medicine* **2021**, *27* (4), 601−615.

(13) World Health Organization. *A clinical case definition of post COVID-19 condition by a Delphi consensus*; WHO, 2021; https://www.who.int/publications/i/item/WHO-2019-nCoV-Post_COVID-19_condition-Clinical_case_definition-2021.1 (accessed June 2023).

(14) Ranucci, M.; Baryshnikova, E.; Anguissola, M.; Pugliese, S.; Falco, M.; Menicanti, L. The Long Term Residual Effects of COVID-Associated Coagulopathy. *International Journal of Molecular Sciences* **2023**, *24* (6), 5514.

(15) Turner, S.; Khan, M. A.; Putrino, D.; Woodcock, A.; Kell, D. B.; Pretorius, E. Long COVID: pathophysiological factors and abnormalities of coagulation. *Trends in Endocrinology & Metabolism* **2023**, *34* (6), 321−344.

(16) Thompson, R. C.; Simons, N. W.; Wilkins, L.; Cheng, E.; Del Valle, D. M.; Hoffman, G. E.; Cervia, C.; Fennessy, B.; Mouskas, K.; Francoeur, N. J.; et al. Molecular states during acute COVID-19 reveal distinct etiologies of long-term sequelae. *Nature Medicine* **2023**, *29* (1), 236−246.

(17) Rahi, M. S.; Parekh, J.; Pednekar, P.; Mudgal, M.; Jindal, V.; Gunasekaran, K. Role of Therapeutic Anticoagulation in COVID-19: The Current Situation. *Hematology Reports* **2023**, *15* (2), 358−369.

(18) Russell, C. D.; Lone, N. I.; Baillie, J. K. Comorbidities, multimorbidity and COVID-19. *Nature Medicine* **2023**, *29* (2), 334−343.

(19) Ackermann, M.; Verleden, S. E.; Kuehnel, M.; Haverich, A.; Welte, T.; Laenger, F.; Vanstapel, A.; Werlein, C.; Stark, H.; Tzankov, A.; et al. Pulmonary Vascular Endothelialitis, Thrombosis, and Angiogenesis in Covid-19. *N Engl J. Med.* **2020**, *383* (2), 120−128.

(20) Grobbelaar, L. M.; Venter, C.; Vlok, M.; Ngoepe, M.; Laubscher, G. J.; Lourens, P. J.; Steenkamp, J.; Kell, D. B.; Pretorius, E. SARS-CoV-2 spike protein S1 induces fibrin(ogen)

resistant to fibrinolysis: implications for microclot formation in COVID-19. *Biosci Rep* **2021**, *41* (8), BSR20210611.
(21) Perico, L.; Benigni, A.; Casiraghi, F.; Ng, L. F. P.; Renia, L.; Remuzzi, G. Immunity, endothelial injury and complement-induced coagulopathy in COVID-19. *Nature Reviews Nephrology* **2021**, *17* (1), 46−64.
(22) Luzak, B.; Rozalski, M.; Przygodzki, T.; Boncler, M.; Wojkowska, D.; Kosmalski, M.; Watala, C. SARS-CoV-2 Spike Protein and Neutralizing Anti-Spike Protein Antibodies Modulate Blood Platelet Function. *International Journal of Molecular Sciences* **2023**, *24* (6), 5312.
(23) Venter, C.; Bezuidenhout, J. A.; Laubscher, G. J.; Lourens, P. J.; Steenkamp, J.; Kell, D. B.; Pretorius, E. Erythrocyte, Platelet, Serum Ferritin, and P-Selectin Pathophysiology Implicated in Severe Hypercoagulation and Vascular Complications in COVID-19. *Int. J. Mol. Sci.* **2020**, *21* (21), 8234.
(24) Lee, M.-H.; Perl, D. P.; Nair, G.; Li, W.; Maric, D.; Murray, H.; Dodd, S. J.; Koretsky, A. P.; Watts, J. A.; Cheung, V.; et al. Microvascular Injury in the Brains of Patients with Covid-19. *New England Journal of Medicine* **2021**, *384* (5), 481−483.
(25) De Michele, M.; d'Amati, G.; Leopizzi, M.; Iacobucci, M.; Berto, I.; Lorenzano, S.; Mazzuti, L.; Turriziani, O.; Schiavo, O. G.; Toni, D. Evidence of SARS-CoV-2 spike protein on retrieved thrombi from COVID-19 patients. *J. Hematol Oncol* **2022**, *15* (1), 108.
(26) Pretorius, E.; Venter, C.; Laubscher, G. J.; Lourens, P. J.; Steenkamp, J.; Kell, D. B. Prevalence of readily detected amyloid blood clots in 'unclotted' Type 2 Diabetes Mellitus and COVID-19 plasma: a preliminary report. *Cardiovasc Diabetol* **2020**, *19* (1), 193.
(27) Wool, G. D.; Miller, J. L. The Impact of COVID-19 Disease on Platelets and Coagulation. *Pathobiology* **2021**, *88* (1), 15−27.
(28) Gąsecka, A.; Borovac, J. A.; Guerreiro, R. A.; Giustozzi, M.; Parker, W.; Caldeira, D.; Chiva-Blanch, G. Thrombotic Complications in Patients with COVID-19: Pathophysiological Mechanisms, Diagnosis, and Treatment. *Cardiovascular Drugs and Therapy* **2021**, *35* (2), 215−229.
(29) Collett, L. W.; Gluck, S.; Strickland, R. M.; Reddi, B. J. Evaluation of coagulation status using viscoelastic testing in intensive care patients with coronavirus disease 2019 (COVID-19): An observational point prevalence cohort study. *Australian Critical Care* **2021**, *34* (2), 155−159.
(30) Pretorius, E.; Lipinski, B. Differences in Morphology of Fibrin Clots Induced with Thrombin and Ferric Ions and Its Pathophysiological Consequences. *Heart Lung Circ* **2013**, *22* (6), 447−449.
(31) Pretorius, E.; Mbotwe, S.; Bester, J.; Robinson, C. J.; Kell, D. B. Acute induction of anomalous and amyloidogenic blood clotting by molecular amplification of highly substoichiometric levels of bacterial lipopolysaccharide. *Journal of The Royal Society Interface* **2016**, *13* (122), No. 20160539.
(32) Han, K.; Zhou, W.; Ma, S.; Wang, S.; Qi, X.; Guo, L.; Li, X. A computational study of fibrinogen-induced alteration in microvascular blood flow in COVID-19. *European Physical Journal Special Topics* **2023**, *232*, 2761.
(33) Baker, S. R.; Halliday, G.; Ząbczyk, M.; Alkarithi, G.; Macrae, F. L.; Undas, A.; Hunt, B. J.; Ariëns, R. A. S. Plasma from patients with pulmonary embolism show aggregates that reduce after anticoagulation. *Communications Medicine* **2023**, *3* (1), 12.
(34) Kruger, A.; Vlok, M.; Turner, S.; Venter, C.; Laubscher, G. J.; Kell, D. B.; Pretorius, E. Proteomics of fibrin amyloid microclots in long COVID/post-acute sequelae of COVID-19 (PASC) shows many entrapped pro-inflammatory molecules that may also contribute to a failed fibrinolytic system. *Cardiovascular Diabetology* **2022**, *21* (1), 190.
(35) Zuo, Y.; Estes, S. K.; Ali, R. A.; Gandhi, A. A.; Yalavarthi, S.; Shi, H.; Sule, G.; Gockman, K.; Madison, J. A.; Zuo, M. Prothrombotic autoantibodies in serum from patients hospitalized with COVID-19. *Sci. Transl Med.* **2020**, *12* (570), eabd3876.
(36) Laubscher, G. J.; Lourens, P. J.; Venter, C.; Kell, D. B.; Pretorius, E. TEG((R)), Microclot and Platelet Mapping for Guiding Early Management of Severe COVID-19 Coagulopathy. *J. Clin Med.* **2021**, *10* (22), 5381.
(37) Bergaglio, T.; Bhattacharya, S.; Thompson, D.; Nirmalraj, P. N. Label-Free Digital Holotomography Reveals Ibuprofen-Induced Morphological Changes to Red Blood Cells. *ACS Nanoscience Au* **2023**, *3* (3), 241−255.
(38) Virkler, K.; Lednev, I. K. Raman spectroscopic signature of blood and its potential application to forensic body fluid identification. *Anal Bioanal Chem.* **2010**, *396* (1), 525−534.
(39) Atkins, C. G.; Buckley, K.; Blades, M. W.; Turner, R. F. B. Raman Spectroscopy of Blood and Blood Components. *Appl. Spectrosc.* **2017**, *71* (5), 767−793.
(40) Blat, A.; Dybas, J.; Chrabaszcz, K.; Bulat, K.; Jasztal, A.; Kaczmarska, M.; Pulyk, R.; Popiela, T.; Slowik, A.; Malek, K.; et al. FTIR, Raman and AFM characterization of the clinically valid biochemical parameters of the thrombi in acute ischemic stroke. *Sci. Rep* **2019**, *9* (1), 15475.
(41) Mihalko, E.; Brown, A. C. Clot Structure and Implications for Bleeding and Thrombosis. *Semin Thromb Hemost* **2020**, *46* (1), 96−104.
(42) Weisel, J. W. Structure of fibrin: impact on clot stability. *Journal of Thrombosis and Haemostasis* **2007**, *5*, 116−124.
(43) Pollaro, L.; Equis, S.; Dalla Piazza, B.; Cotte, Y. Stain-free 3D Nanoscopy of Living Cells. *Optik & Photonik* **2016**, *11*, 38−42.
(44) Wassie, A. T.; Zhao, Y.; Boyden, E. S. Expansion microscopy: principles and uses in biological research. *Nat. Methods* **2019**, *16* (1), 33−41.
(45) Iba, T.; Levy, J. H. A commentary on "Thromboinflammation in long COVID − the elusive key to post-infection sequelae? *Journal of Thrombosis and Haemostasis* **2023**, *21* (8), 2061−2063.
(46) Zhang, H.; Zang, C.; Xu, Z.; Zhang, Y.; Xu, J.; Bian, J.; Morozyuk, D.; Khullar, D.; Zhang, Y.; Nordvig, A. S.; et al. Data-driven identification of post-acute SARS-CoV-2 infection subphenotypes. *Nature Medicine* **2023**, *29* (1), 226−235.
(47) Nirmalraj, P. N.; Schneider, T.; Lüder, L.; Felbecker, A. Protein fibril length in cerebrospinal fluid is increased in Alzheimer's disease. *Commun. Biol.* **2023**, *6* (1), 251.
(48) Phillips, K. G.; Jacques, S. L.; McCarty, O. J. T. Measurement of Single Cell Refractive Index, Dry Mass, Volume, and Density Using a Transillumination Microscope. *Phys. Rev. Lett.* **2012**, *109* (11), No. 118105.
(49) Friebel, M.; Meinke, M. Model function to calculate the refractive index of native hemoglobin in the wavelength range of 250−1100 nm dependent on concentration. *Appl. Opt.* **2006**, *45* (12), 2838−2842.

https://doi.org/10.1021/cbmi.3c00126
Chem. Biomed. Imaging XXXX, XXX, XXX−XXX